

Nonlinear statistical characteristics of the multi-directional waves with equivalent energy

Lei Wang (王磊)^{a,c}, Kanglixi Ding (丁康礼玺)^a, Binzhen Zhou (周斌珍)^{a,*}, Peng Jin (金鹏)^b, Shuxue Liu (柳淑学)^c,
Jinghua Wang (王菁华)^d, Tianning Tang (唐天宁)^e

^a School of Civil Engineering and Transportation, South China University of Technology, Guangzhou 510641, China

^b School of Marine Science and Engineering, South China University of Technology, Guangzhou 510641, China

^c State Key Laboratory of Coastal and Offshore Engineering, Dalian University of Technology, Dalian 116024, China

^d Department of Civil and Environmental Engineering, The Hong Kong Polytechnic University, Hong Kong, 999077, China

^e Department of Engineering Science, University of Oxford, Oxford, OX1 3PJ, United Kingdom

Abstract

Directional distribution is believed to have a significant impact on the statistical characteristics in multi-directional sea states. In real sea states, short-crested waves are discrete not only in frequency but also in direction. For the former one, they are well explained in unidirectional mode, but for the latter one, they are not. In this paper, the kurtosis of short-crested waves with equivalent energy is first discussed. Unimodal-spectrum-multi-direction sea states and bimodal-spectrum-multi-direction sea states are simulated for a long time in a numerical wave basin based on High Order Spectral (HOS) method. In the equivalent sea-swell sea state, the spatial evolution of kurtosis becomes more inhomogeneous, along with the maximum value of kurtosis being larger and the area where the maximum value occurs wider in the configuration with a crossing angle $\beta=40^\circ$ than that with $\beta=0^\circ$, while little variations in swell-dominated and wind-sea-dominated states. A positive linear correlation between wavelet group steepness and kurtosis is obtained in a unimodal sea state, but not applied to a crossing sea state characterized by a bimodal spectrum. The exceedance probability of wave height and wave crest distribution at maximum kurtosis are also given. These findings can help predict the probability of extreme waves occurring, guiding the selection of ocean engineering sites to avoid extreme configurations.

Keywords: High Order Spectral method, exceedance probability of wave height, kurtosis, multi-directional waves, crossing sea states

1. Introduction

Kurtosis, defined as the fourth moment of the free surface elevation, is introduced as an indication of extreme events [1][2]. In the real sea state, oceanic waves are featured with multi-directional characteristics [3]-[5], which are proven to have a great effect on wave evolution [6][7]. For a narrower directional spectrum, nonlinear modulation instability plays a dominant role, while as the directional distribution widens, resonance dominates causing a redistribution of the energy spectrum. However, in most previous literature, ocean waves were simplified to be unidirectional [8]-[10] to determine the conservative thresholds of the extreme configuration, leaving out the significant role of directional distribution. Therefore, investigating nonlinear statistics such as kurtosis in multi-directional sea states is quite essential for promoting the prediction of extreme wave occurrence in practical engineering.

Great efforts have been advanced in the statistical property of unidirectional waves. According to the linear

* Corresponding authors
E-mail address: zhoubinzhen@scut.edu.cn (B. Zhou)

theory, the propagation of surface gravity waves was regarded as a Gaussian process [11]. Under the assumption of a narrow band, the wave height was twice the envelop amplitude. The wave height distribution obeyed the Rayleigh distribution, and so did the crest distribution [12]. The linear theory was successfully applied to some given circumstances such as the dissipation of swell wave [13], abrupt depth transfer [14], the attenuation due to an inextensible cover [15], and so on. However, linear theory cannot accurately capture the changes in free surface elevation and wave dispersion due to high-order harmonic interactions, which is crucial for the nonlinear statistical characteristics. The nonlinear theory was consequently put forward. Modulation instability, also known as third-order interactions, was found to affect the tail of the exceedance probability of wave height distribution [16]. Later, a ratio between the wave steepness and the relative spectral bandwidth named Benjamin-Feir Index (BFI) was proposed to measure the strength of third-order interactions [17]. A sequence of research showed that Rayleigh distribution underestimated the statistical tail of the exceedance probability for the wave configuration with a larger BFI. And the larger the BFI, the greater the deviation from the Rayleigh distribution [2]. Kurtosis was further proven to be relevant to the nonlinear correction to large wave height distribution [18]. By introducing kurtosis as a correction to the Rayleigh distribution, the modified Edgeworth-Rayleigh distribution (MER) came up [19]. Although the hypothesis of the weakly nonlinear model was narrow-banded, MER distribution was widely approved in dealing with some extreme waves. Li and Li [20] developed a semi-analytical approach to describe the weakly nonlinear broad-banded multi-directional water waves, promoting the accuracy of large wave predictions.

Directional distribution has been proven to transform the physical mechanism in the process of water wave evolution [21]-[23]. The impact of the directional distribution cannot be ignored. In a multi-directional sea state under unimodal configuration, it was mathematically deduced that narrower direction distribution was prone to triggering much more extreme waves [24]. Onorato et al. [25] experimentally simulated unimodal waves considering directional distribution width ranging from 0° to $\pm 30^\circ$. The occurrence probability of large waves was observed to be close to the second-order wave theory. Except for the most commonly studied unimodal sea state, bimodal spectral sea state has also attracted more attention [26][27]. The well-known extreme event "New Year Wave" [28] as well as the catastrophic accident of Louis Majesty [29] was theoretically proved to occur in the mixed system by reconstructing the wave field. Onorato et al. [30] deduced a coupled nonlinear Schrödinger (CNLS) equation considering the same wave train crossed and found that there were larger regions and larger growth rates of instability in coupled systems, which was also found by Grönlund et al. [31]. Regev et al. [32] pointed out that a weak swell across into a wind-sea system at a right angle can promote extreme wave occurrence. Followed by this, Gramstad and Trulsen [33] also conducted the statistics of a wind-sea system perturbed by a weak swell oriented at various angles and observed that the addition of a swell system enhanced the instability of the wind-sea system slightly. The kurtosis was to be found to increase in the crossed sea state at a crossing angle between 40° and 60° [34].

In real sea states, surface gravity waves are discrete not only in frequency but also in direction. For the former one, they are well explained in unidirectional mode, but for the latter one, they are not. Further, the sea states with equal significant wave height or with the same wind-sea system have been extensively summarized, but the sea states with equivalent energy but different energy distributions are not studied. The influence of directional distribution and energy distribution in crossing bimodal sea states on nonlinear statistics is still unknown. Therefore, two types of spectral configurations in multi-directional sea state are going to be numerically simulated and the corresponding effect will be explored in this study. The novelties of our work are three-folded. First, the spatial evolution of kurtosis in crossing sea states is firstly investigated. The influence of the crossing angle on kurtosis variation is associated with energy distribution. Second, the relation of wave group steepness based on wavelet transform and kurtosis in a multi-directional sea state is summarized. Third, two dominant

indexes of extreme events, the exceedance probability of wave height distribution and wave crest distribution, are compared at maximum kurtosis rather than at the preset position in different configurations.

The rest of the paper is arranged as follows. Section 2 describes the multi-directional sea state. The numerical model based on High Order Spectral (HOS) method is established in Section 3, also with the introduction of analytical parameters used. Nonlinear statistical characteristics in unimodal sea state and crossing sea state are analyzed in Section 4.

2. Multi-directional sea state

Waves are directionally spread in the real sea state. Whereas, multi-directional features are usually ignored and simplified as unidirectional in most previous literature. In this study, two types of multi-directional configurations under the assumption of equivalent energy are going to be investigated: unimodal-spectrum-multi-direction sea state (also abbreviated to unimodal sea state in the following context) and bimodal-spectrum-multi-direction sea state (also abbreviated to crossing sea state).

2.1 Wave boundary condition

The expected free surface elevation $\eta_{\text{expected}}(x, y, t)$ of multi-directional waves at position (x, y) in a given sea state can be expressed as

$$\eta_{\text{expected}}(x, y, t) = \sum_{i=1}^{N_f} \sum_{j=1}^{N_\theta} a_{ij} \cos[k_{ij}(x \cos \theta_j + y \sin \theta_j) - 2\pi f_{ij}t + \varphi_{ij}] \quad (1)$$

where N_f and N_θ are the total number of the division in the prescribed spectral range $[f_L, f_H]$ and the directional range $[\theta_{\min}, \theta_{\max}]$, respectively. θ_j denotes the included angle between the main wave direction θ_0 and the x -axis, defining the counterclockwise direction as positive. φ_{ij} represents the initial random phase uniformly distributed within the range of $[0, 2\pi]$. f_{ij} and k_{ij} are the frequency and wavenumber of the i -th spectral and j -th directional wave components, respectively. To avoid the waves reoccurring periodically, the division method in the spectral and directional range is used as follows

$$f_{ij} = f'_i - \frac{1}{2} \Delta f + (j-1 + \text{RAN}_{ij}) \Delta f / N_\theta \quad (2)$$

$$\Delta f = (f_H - f_L) / N_f; \quad f'_i = f_L + (i-1) \Delta f$$

$$\theta_j = \theta_{\min} + (j-1) \Delta \theta \quad (3)$$

$$\Delta \theta = (\theta_{\max} - \theta_{\min}) / N_\theta$$

where RAN_{ij} is a random number uniformly distributed in the range of $[0, 1]$.

Wave amplitude a_{ij} can be calculated by

$$a_{ij} = \sqrt{2S(f_{ij}, \theta_j) \Delta f \Delta \theta} \quad (4)$$

in which the directional spectrum $S(f, \theta)$ is defined as the product of the frequency spectrum $S(f)$ and the directional distribution function $G(\theta)$

$$S(f_{ij}, \theta_j) = S(f_j) G(\theta_j) \quad (5)$$

2.2 Frequency spectrum

Frequency spectrum $S(f)$ proposed by Ochi and Hubble [35], which can represent the mixed sea state composed of swell and wind-sea, is adopted in this study.

$$S(f) = \frac{1}{4} \sum_j \frac{\left(\frac{4\lambda_j+1}{4}\right)^{\lambda_j}}{\Gamma(\lambda_j)} \left(\frac{f_{\theta}}{f}\right)^{4\lambda_j} \frac{H_{\theta}^2}{f} \exp\left[-\frac{4\lambda_j+1}{4} \left(\frac{f_{\theta}}{f}\right)^4\right] \quad j=1, 2 \quad (6)$$

where $j=1, 2$ represent the low-frequency and high-frequency parts, respectively, which in turn correspond to the swell and wind-sea in the mixed system, respectively. Γ is the gamma function. Each part has three parameters respectively, i.e., the significant wave height H_s , the spectral peak angular frequency ω_p ($=2\pi f_p$), and the peak enhancement factor λ .

In the simulation of different sea states to investigate the impact of spectral distribution on nonlinear effect in multi-directional sea states, the total wave energy remains unchanged, which is weighed by the mean zero-crossing period T_z . It is fixed at 0.80s in the following study. This characteristic period of the mixed system is defined as

$$\sqrt{\frac{H_{s1}^2 + H_{s2}^2}{H_{s1}^2/T_{z1}^2 + H_{s2}^2/T_{z2}^2}} = T_z \quad (7)$$

$$T_{z1} = 2\pi \sqrt{\frac{m_{01}}{m_{21}}} \quad T_{z2} = 2\pi \sqrt{\frac{m_{02}}{m_{22}}} \quad (8)$$

where m_0 and m_2 are the zero- and second-order spectral moment, respectively.

2.3 Directional distribution function

Assuming the main wave direction of the simulated waves as θ_0 , the directional distribution function $G(\theta)$ is adopted as the method proposed by Longuet-Higgins et al. [36], defined as

$$G(\theta) = \frac{\cos^{2s}\left(\frac{\theta-\theta_0}{2}\right)}{\sum_1^{N_s} \cos^{2s}\left(\frac{\theta-\theta_0}{2}\right)} \quad (9)$$

where s is the directional spreading parameter.

The variation of the directional distribution function $G(\theta)$ with directional spreading parameters s under the assumption of the main wave direction θ_0 equal to 0, is given in Fig. 1.

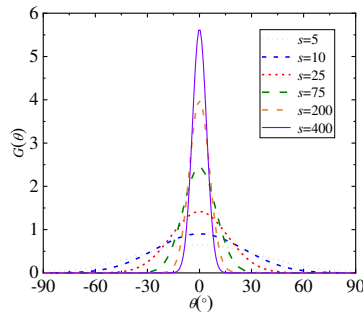


Fig. 1 Variation of the directional distribution function with directional spreading parameters.

The directional distribution width is consequently defined as the standard deviation of the spreading distribution σ_θ to measure the directional distribution of multi-directional waves, induced as [37]

This is the author's peer reviewed, accepted manuscript. However, the online version of record will be different from this version once it has been copyedited and typeset.

PLEASE CITE THIS ARTICLE AS DOI: 10.1063/5.0160775

$$\sigma_{\theta} = \left\{ \int_{-\frac{\pi}{2}}^{\frac{\pi}{2}} G(f, \theta) (\theta - \theta_0)^2 d\theta \right\}^{\frac{1}{2}} \quad (10)$$

The relation of the wave directional distribution width σ_{θ} with the directional spreading parameter s is illustrated in Fig. 2. As s increases, σ_{θ} decreases. For small values of s , the directional distribution width decreases rapidly. But when the value of s is larger than 300, σ_{θ} changes little. At present, the change in s cannot reflect the change in directional distribution width. Therefore, in our following study, the directional spreading parameter s is replaced by the directional distribution width σ_{θ} to describe the directional distribution.

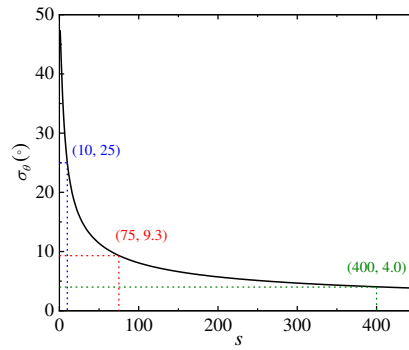


Fig. 2 Variation of the wave directional distribution width with the directional spreading parameter.

2.4 Multi-directional sea state

Two types of multi-directional configurations under the assumption of equivalent energy are going to be investigated: unimodal-spectrum-multi-direction sea state and bimodal-spectrum-multi-direction sea state.

Tab. 1 lists the detailed wave parameters of multi-directional configuration, from unimodal sea states to crossing sea states. In unimodal sea states (Tab. 1a), three cases considering different directional distribution widths are tested for reference, in which BFI denotes the deep-water Benjamin-Feir Index (calculated according to Ref. [17]). In crossing sea states (Tab. 1b), the value of Intermodal Distance ($ID = (f_{p2} - f_{p1}) / (f_{p2} + f_{p1})$) [38] is fixed to 0.10, but the value of Sea-Swell Energy Ratio ($SSER = m_{0wind-sea} / m_{0swell}$) [38] is variable, corresponding to sea-swell energy equivalent (Case E), swell-dominated (Case AK) and wind-sea-dominated configuration (Case AO), to investigate the effect of energy distribution on nonlinear statistics. The swell (low-frequency) system with $s=75$ meets the wind-wave (high-frequency) system with $s=25$ at three different crossing angles β ($=|\theta_{01} - \theta_{02}|$, θ_{01} and θ_{02} represent the main wave direction of the swell system and the wind-wave system, respectively).

Concerning the information of wave components, the total number of the division in the spectral and directional range is consistent with $N_f=200$ and $N_{\theta}=100$, the prescribed spectral and directional range is taken as $[f_L, f_H]=[0.2 \text{ Hz}, 3.0 \text{ Hz}]$ and $[\theta_{min}, \theta_{max}]=[-90^{\circ}, 90^{\circ}]$.

Tab. 1 Detailed parameters of two types of multi-directional wave configuration ($h=4 \text{ m}$)

(a) unimodal sea state						
Case	f_p (Hz)	H_s (m)	BFI= $\sqrt{2\varepsilon} / (2\Delta f / f_p)$	s	σ_{θ} ($^{\circ}$)	θ_0 ($^{\circ}$)

Case unimodal	0.8	0.0469	0.6	10, 75, 400	25, 9.3, 4.0	0
---------------	-----	--------	-----	-------------	--------------	---

1

(b) crossing sea state (ID=0.10)					
Case	f_p (Hz)	H_s (m)	SSER	s	$\beta= \theta_{01}-\theta_{02} $ ($^\circ$)
Case E	0.90	0.0212	1.00	75	0, 20, 40
	1.09	0.0212		25	
Case AK	0.98	0.0287	0.09	75	
	1.20	0.0087		25	
Case AO	0.85	0.0141	3.66	75	
	1.04	0.0265		25	

2

3

4

5

6

7

8

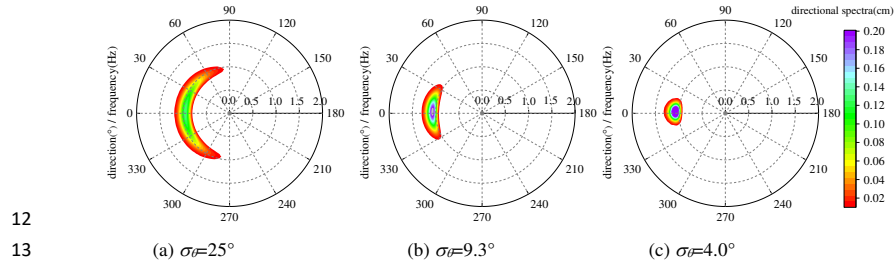
9

10

11

Fig. 3 and Fig. 4 show the directional spectra of multi-directional configuration, including the unimodal sea states and the crossing sea states, illustrating the energy distribution of each wave component in directional (along the circular arc direction) and in spectral (along the radial direction) range.

In unimodal sea states (Fig. 3), the wave energy mainly focused in the spectral range of 0.7 Hz -1.0 Hz is symmetrically distributed on both sides of the main wave direction. As the directional distribution narrows, the wave energy becomes more concentrated in the main wave direction. Till $\sigma_f=4.0^\circ$, the wave energy is concentrated in a quite narrow width, approaching the status of the unidirectional sea state. In crossing sea states (Fig. 4), when the two systems with concentrated energy meet at different crossing angles, the directional distribution widths of the mixed sea states are variable. With the increase of the crossing angles β , the directional distribution becomes wider, along with the concentrated wave energy deviated from 0° to $\pm 20^\circ$.



12

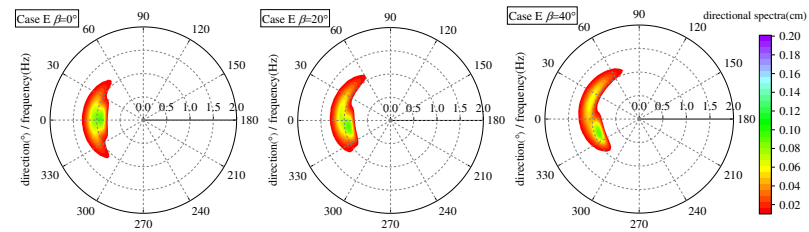
13

14

Fig. 3 Directional spectra of the unimodal sea states considering various directional distribution widths.

15

16



(a) sea-swell energy equivalent (Case E, SSER=1.0)

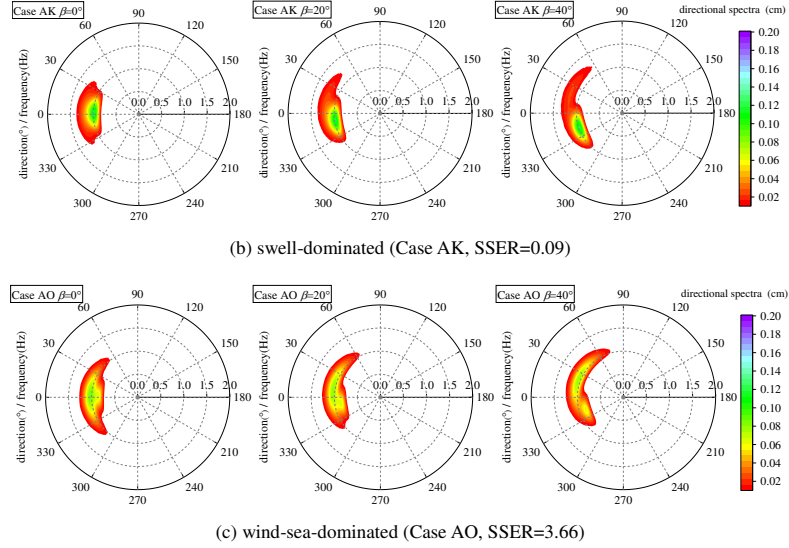


Fig. 4 Directional spectra of the crossing sea states considering various crossing angles.

3. Numerical set-up and analytical parameters

3.1 Numerical model

The numerical wave basin employed in the following analysis is illustrated in Fig. 5. It includes a wavemaker and three absorbing zones. Limited to the effective simulation area (a triangle shown in Fig. 5a) influenced by the directional distribution of the expected waves, the numerical domain is assumed as 130 m long and 200 m wide to ensure sufficient wave evolution. The origin of the coordinate is set at the wavemaker center, with the x -axis along the centerline of the numerical wave basin and the y -axis along the wavemaker. The water depth is 4.0 m. A sequence of wave gauges (represented as solid dots) is arranged in the wave field to record the free surface elevations, shown in Fig. 5b. The wave gauges are arranged every 5 m along the centerline (i.e., Y_0) and the parallel distanced 20 m and 40 m from the centerline both in upper and lower sides (i.e., $Y_{\pm 20}$ and $Y_{\pm 40}$), and every 10 m along the parallel distanced 10 m and 30 m from the centerline both in upper and lower sides (i.e., $Y_{\pm 10}$ and $Y_{\pm 30}$). An array of wave gauges is involved to verify the input directional spectrum.

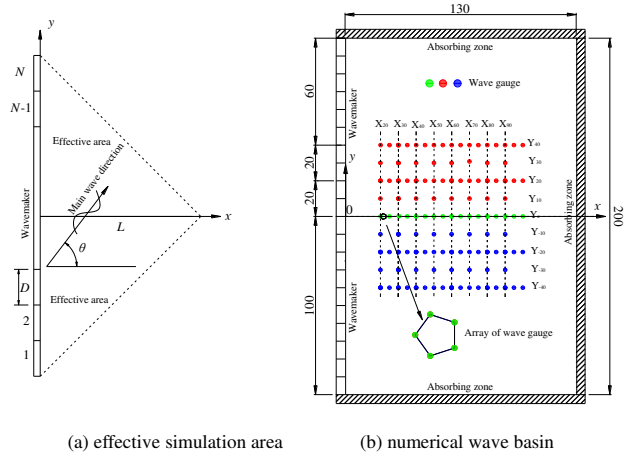


Fig. 5 Layout of numerical wave basin for multi-directional simulation (unit: m)

The High Order Spectral (HOS) method is used to solve the numerical model for higher efficiency in three-dimensional simulation with full nonlinearity persisted. Based on the potential flow theory, the numerical method introducing the non-periodic boundary condition can be solved with the velocity potential being split into the sum of two-folded potential. The free-surface spectral potential component Φ_f can be solved by the original HOS method in which the velocity potential is written in a perturbation series up to an arbitrary order, and the prescribed non-periodic component Φ_w can be expressed as another set of specific basis functions. More supplementary details of the numerical solution can be referred to Refs. [39][40] and Appendix.

Convergence analysis of the HOS numerical model conducted in Ref. [40] proposes that the number of points per peak wavelength can be adopted as 30, the time step is 1/100 of the wave period, and the order of the HOS method is 5. These discretizations will be used in the coming numerical simulation. As in the method adopted before, ten random seeds different from each other are to be chosen for more universal results (the convergence analysis concerning the random seed can be referred to Fig. 4 in Ref. [41]), and at least 5000 waves are ensured to be effectively collected by all gauges in each wave configuration.

3.2 Model validation

The numerical model based on the HOS method has been validated by Wang et al. [40] and Ducroz et al. [42]. Here the input conditions for multi-directional waves need additional verification by comparing them with the theoretical values. Fig. 6 and Fig. 7 give the comparison of wave spectra $S(f)$ and direction distributions $G(\theta)$. The numerically simulated results using the HOS method at 10m away from the wavemaker are in good agreement with the theoretical values in various multi-directional sea states, proving that the HOS numerical wave basin established in this study can be adapted to accurately simulate multi-directional waves.

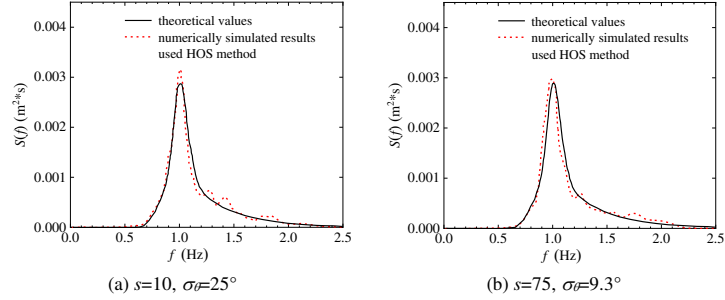


Fig. 6 Comparison of wave spectra between measured results and theoretical values.

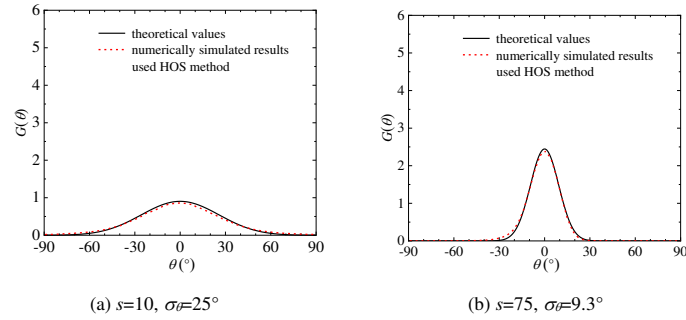


Fig. 7 Comparison of directional distributions between measured results and theoretical values.

3.3 Analytical parameters

Nonlinear statistical parameters are commonly used to reveal the non-Gaussian characteristics of the sea states. The parameters analyzed later are to be introduced as follows.

3.3.1 Kurtosis

Kurtosis, defined as the fourth moment around the mean divided by the square of the average surface elevation variance σ^2 , is expressed as

$$kurtosis = \frac{\langle (\eta - \langle \eta \rangle)^4 \rangle}{\sigma^4} \quad (11)$$

3.3.2 Wave group parameters

Wave group parameters can reflect some local characteristics of the sea states that cannot be described by wave elements or spectral parameters. Resemble to wave steepness, wave group steepness (i.e., GF_W/GL_W) is defined as a ratio of group height factor GF_W and group length factor GL_W , which are obtained based on wavelet energy history [43]. This time-frequency analysis method can help capture the frequency characteristics in a local range in dealing with strongly nonlinear transient signals.

The refined group height factor GF_W is

$$GF_W = \frac{1}{\overline{W(t)}} \sqrt{\frac{1}{T_n} \int_0^{T_n} [W(t) - \overline{W(t)}]^2 dt} \quad (12)$$

1 where $\overline{W(t)}$ is the period-averaged wavelet energy history $W(t)$. The history of wavelet energy is expressed as

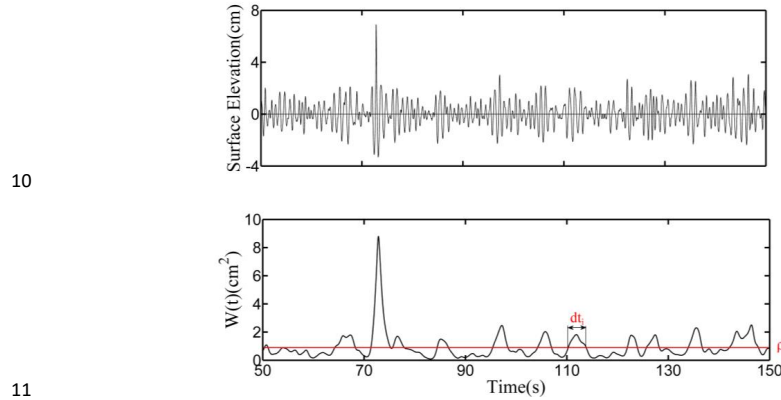
$$2 \quad W(t) = \frac{\delta \Delta t}{C_\delta} \int_0^\infty \frac{|WT(\tau, s)|^2}{s} ds \quad (13)$$

3 where C_δ is the reconstruction coefficient.

4 The group length factor GL_W is redefined as

$$5 \quad GL_W = \frac{1}{N} \sum_{i=1}^N dt_i f_{pi} \quad (14)$$

6 where N is the number of wave groups in the analyzed wave train, dt_i is the time duration, and f_{pi} is the spectral
7 peak frequency of the i -th wave group, respectively, illustrated in Fig. 8. dt_i approximately equal to the
8 wavenumber of the i -th wave group, depending on the selection of the threshold value ρ . Here ρ is adopted as
9 the period-averaged wavelet energy history.



10
11 Fig. 8 Time series and its wavelet energy of one wave train.

12 3.3.3 Exceedance probability of wave height

13 (a) Rayleigh distribution

14 In a stationary, Gaussian, and extremely narrow banded process, the wave height distribution obeys the
15 Rayleigh distribution [12] under the assumption that the wave height is twice the envelope amplitude.

$$16 \quad E(H) = \exp \left[-\frac{H^2}{8m_0} \right] \quad (15)$$

17 where $m_0 = H^2/4$ is the zero-order spectral momentum.

18 (b) MER distribution

19 Introducing weakly nonlinear interaction, the modified Edgeworth-Rayleigh distribution (MER) can predict
20 the wave height distribution in a narrow banded process, defined as [19]:

$$21 \quad E(H) = \exp \left(-\frac{H^2}{8m_0} \right) \left[1 + \left(\text{kurtosis} - 3 \right) \frac{H^2}{384m_0} \left(\frac{H^2}{m_0} - 16 \right) \right] \quad (16)$$

3.3.4 Exceedance probability of wave crest

(a) Rayleigh distribution

The wave height of the Gaussian sea state theoretically conforms to Rayleigh distribution [12]

$$E(\eta_c) = 1 - \exp \left[-8 \left(\frac{\eta_c}{H_s} \right)^2 \right] \quad (17)$$

(b) Forristall distribution

A wave crest distribution based on second-order wave theory proposed by Forristall [44] is considered to be applied to unidirectional and multi-directional waves, expressed as:

$$E(\eta_c) = 1 - \exp \left[- \left(\frac{\eta_c}{\alpha_f H_s} \right)^{\beta_f} \right] \quad (18)$$

in which the fitting parameters α_f and β_f can be calculated by

$$\begin{aligned} \alpha_f &= 0.3536 + 0.2568S_1 + 0.0800U_r \\ \beta_f &= 2 - 1.7912S_1 - 0.5302U_r + 0.2840U_r^2 \end{aligned} \quad (19)$$

where S_1 and U_r are the averaged wave steepness and Ursell parameters, respectively. Details can be referred to Ref. [44].

4. Results and analysis

Two types of multi-directional configurations, unimodal-spectrum-multi-direction sea state (abbreviated to unimodal sea state) and bimodal-spectrum-multi-direction sea state (abbreviated to crossing sea state), are going to analyze in this section.

4.1 Overview of the wave field

In the real sea state, the wave fields often appear as multi-directional features, which are usually ignored and simplified as unidirectional. Fig. 9 illustrates the local steady wave fields of the unimodal sea state (Fig. 9a) and crossing sea state (Fig. 9b).

In unimodal sea states (Fig. 9a1-a3), when the directional distribution $\sigma_\theta=25^\circ$ (Fig. 9a1), the free surface elevations present random, without any distinct wave-crest lines. As the width of the directional distribution decreases, the wave trains propagate much more narrowly, along obvious wave crest lines appearing. Till $\sigma_\theta=4.0^\circ$ (Fig. 9a3), there are more wave-crest lines and they are almost parallel to each other, which phenomenon is quite close to a unidirectional sea state. In crossing sea state (Fig. 9b1-b3), the sea-swell energy equivalent configuration is taken as an example. In general, with the increase of the crossing angle β , the wave crest lines become shorter and the energy of the wave trains is less centralized, but the maximum of the wave crest seems larger when $\beta=40^\circ$.

This is the author's peer reviewed, accepted manuscript. However, the online version of record will be different from this version once it has been copyedited and typeset.

PLEASE CITE THIS ARTICLE AS DOI: 10.1063/5.0160775

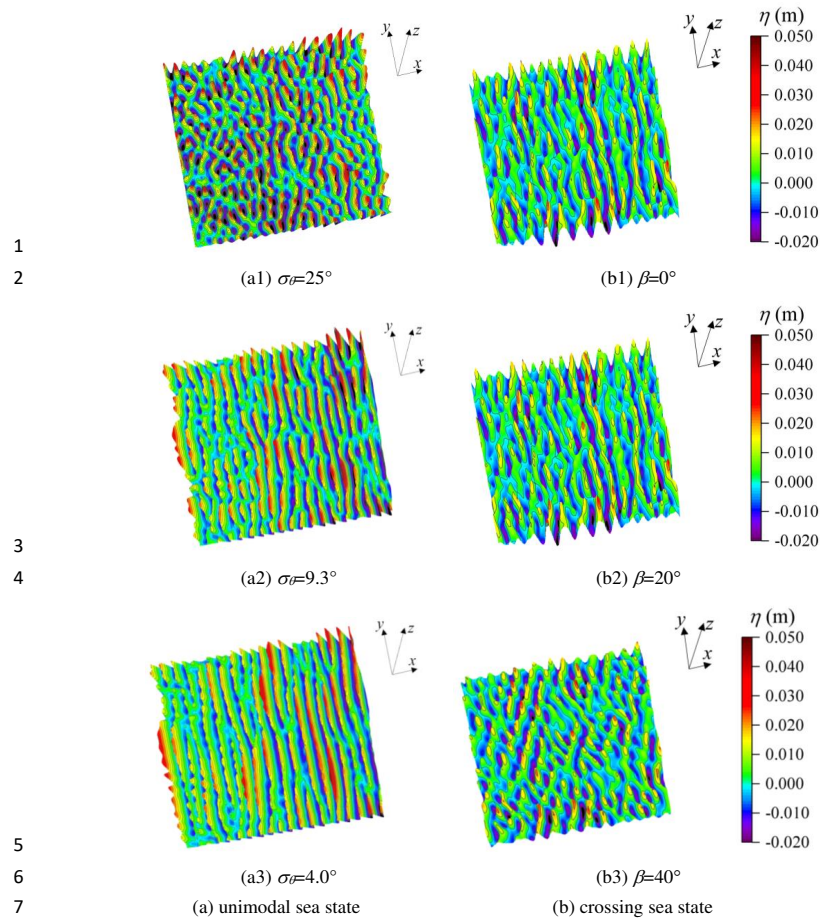


Fig. 9 Local wave field of the unimodal sea state (left: a) and crossing sea state under sea-swell energy equivalent configuration (right: b) in a range of 40 m x 40 m.

4.2 Spatial evolution of kurtosis

As known, kurtosis gradually increases with the wave propagation, then decreases slightly, and finally tends to be stable in a unidirectional sea state [45]. However, in a multi-directional sea state, the spatial evolution of kurtosis is unclear, such as the information on the maximum kurtosis and its corresponding area. Fig. 10 - Fig. 13 give the spatial evolution of kurtosis and its average in unimodal sea state and crossing sea state.

In a unimodal sea state (Fig. 10), the spatial evolution of kurtosis influenced by various direction distribution widths is counted out. With the decrease of directional distribution width, the areas where the maximum value occurs (marked red) become wider and the maximum values of kurtosis in the wave field get larger. This means that there is a greater occurrence probability of large wave events in the unimodal sea state with a narrower directional distribution, due to the stronger instability of the wave trains.

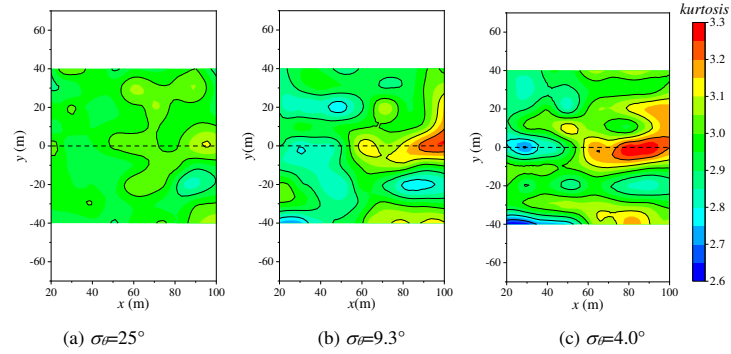


Fig. 10 Spatial evolution of kurtosis in unimodal sea states considering various directional distribution widths.

Fig. 11 compares the average kurtosis along the width direction of the wave basin in unimodal sea states. Besides the absolute value (Fig. 11a), the relative value (Fig. 11b) defined as the percentage of the deviation from the averaged $kurtosis_{ave}$ is also included. When $\sigma_\beta=25^\circ$, the kurtosis along the width direction is around 2.97 except for the one valued at 3.02 on the center line. As the directional distribution width decreases, the greater the deviation from the average and the more positive values. Besides, it is an interesting phenomenon that the maximum of the average kurtosis mainly appears at or near the centerline, explained by the association with the main wave direction.

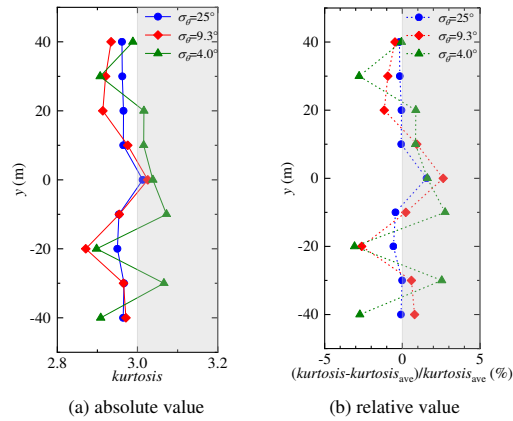


Fig. 11 Average kurtosis along the width direction of the numerical wave basin in unimodal sea states.

Fig. 12 gives the spatial evolution of kurtosis in the crossing sea state considering the effect of the crossing angle. Under the sea-swell equivalent configuration (i.e., SSER=1.0, Fig. 12a), as the crossing angle β increases, the areas where the maximum value occurs become wider, and the maximum values of kurtosis in the wave field get larger, quite similar to the trend of the unimodal state. These results are alike the discoveries of Toffoli et al. [46] that the modulation instability of the mixed system was observed to be greatly increased when the two wave trains met at a crossing angle in the range of 40° - 60° , though the objects are different, that in their study these two wave trains were the same but in ours, they distribute in frequency domain variously. Under the swell-dominated configuration (Fig. 12b), the areas where the maximum value occurs and the maximum values

This is the author's peer reviewed, accepted manuscript. However, the online version of record will be different from this version once it has been copyedited and typeset.

PLEASE CITE THIS ARTICLE AS DOI: 10.1063/5.0160775

of kurtosis in the wave field have no obvious change with the variation of the crossing angle β . Under the wind-sea dominated configuration (Fig. 12c), as the crossing angle β increases, the area where the maximum value occurs decreases slightly and so does the maximum value of kurtosis in the wave field.

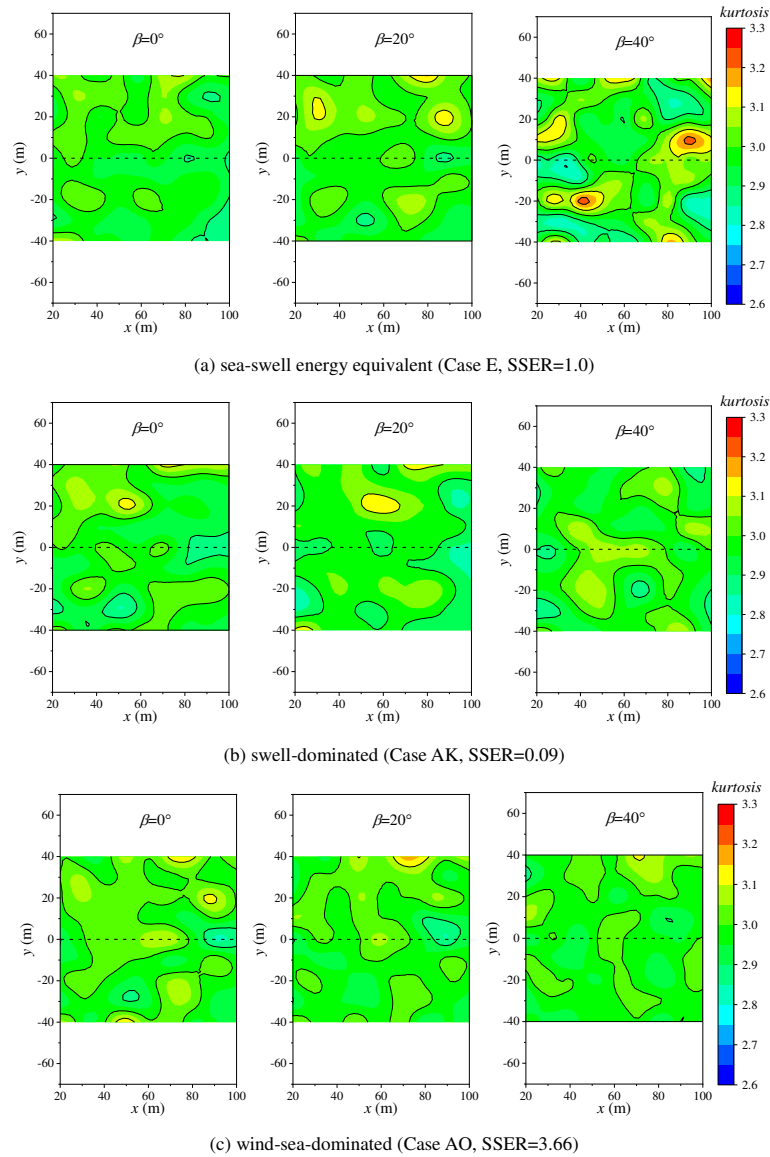
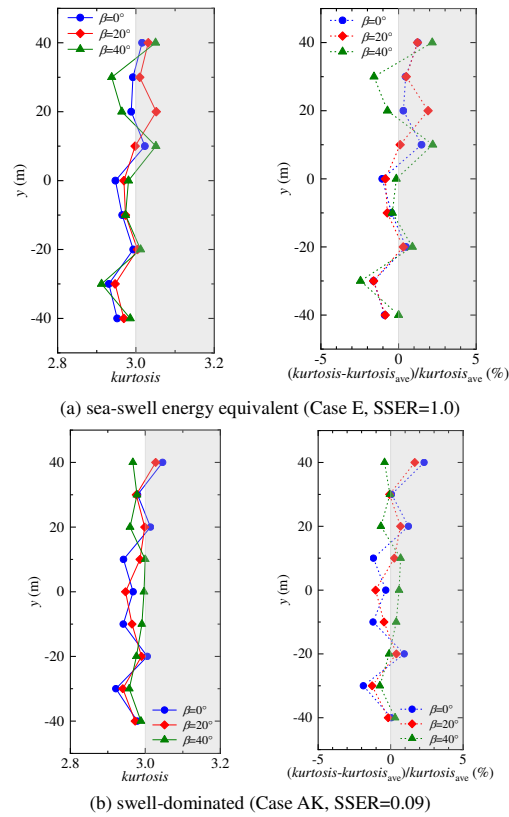


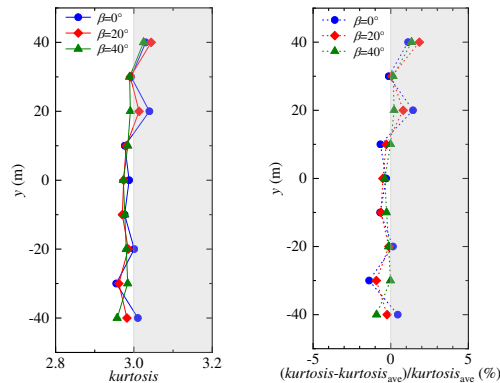
Fig. 12 Spatial evolution of kurtosis in crossing sea states considering various crossing angles.

This is the author's peer reviewed, accepted manuscript. However, the online version of record will be different from this version once it has been copyedited and typeset.

PLEASE CITE THIS ARTICLE AS DOI: 10.1063/5.0160775

Fig. 13 compares the average kurtosis along the width direction of the wave basin in crossing sea states. Comparing the configuration with different energy distributions, the crossing angle has different effects on the variations of kurtosis along the width direction. Under the sea-swell equivalent configuration (Fig. 13a), the larger the crossing angle, the greater the deviations and the more the positive relative values, reflecting that the more inhomogeneous the spatial evolution of kurtosis and the stronger the nonlinearity of the wave field. Moreover, the maximum of the average kurtosis appears away from the centerline, since the main wave direction of the mixed system deviates from the horizontal axis caused by complex nonlinear interactions. Under the energy distribution asymmetric configuration, i.e., swell-dominated (Fig. 13b) or wind-sea-dominated (Fig. 13c), the average kurtosis along the width direction changes a little as the crossing angle varies.





(c) wind-sea-dominated (Case AO, SSER=3.66)

Fig. 13 Average kurtosis along the width direction of the numerical wave basin in crossing sea states (left: absolute value; right: relative value).

4.3 Relation between wave group steepness and kurtosis

Wave group steepness, an important role in describing the local features of a sea state, cannot be ignored in dealing with extreme waves. The relations between wave group steepness GF_W/GL_W and kurtosis in multi-directional sea state are investigated, shown in Fig. 14 and Fig. 15.

In the unimodal sea state (Fig. 14), for the configuration with fixed directional distribution width, the value of kurtosis increases as the group steepness increases, and there is a strong linear correlation between them. As the directional distribution width becomes narrower, the linear relation is hardly affected. Hence, there is a positive linear correlation between wave group steepness and kurtosis irrespective of the directional distribution width.

In crossing sea states (Fig. 15), although the kurtosis increases with the increase of group steepness, the energy distribution has different effects on the correlation between them. Under the sea-swell energy equivalent configuration (Fig. 15a), the wave group steepness and kurtosis satisfy quadratic polynomial regression relation, while under the swell-dominated or wind-sea-dominated configuration (Fig. 15b-c), there is a positive linear relation between wave group steepness and kurtosis, but the growth rates are distinct. This demonstrates that the relation between kurtosis and wave group steepness is not static and it varies with the wave parameters of the given sea state.

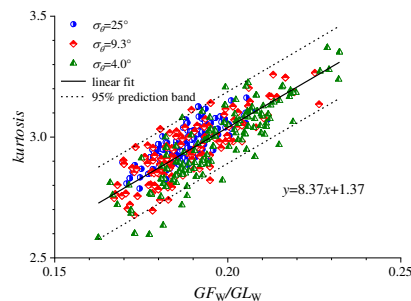
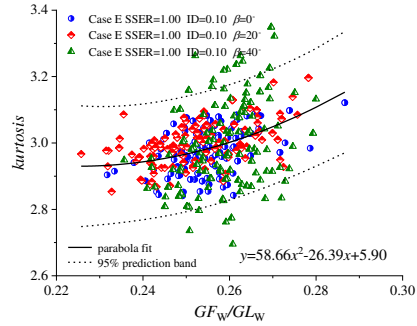


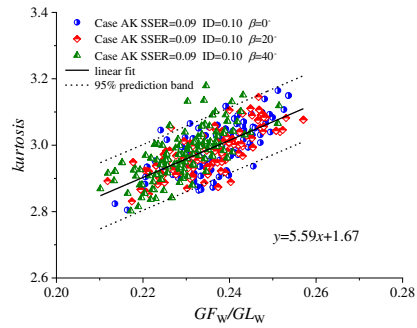
Fig. 14 Relation between wave group steepness and kurtosis in unimodal sea states considering various directional distribution widths.

This is the author's peer reviewed, accepted manuscript. However, the online version of record will be different from this version once it has been copyedited and typeset.

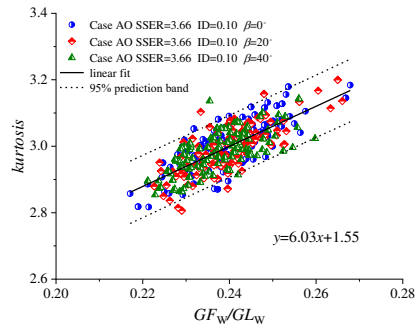
PLEASE CITE THIS ARTICLE AS DOI: 10.1063/5.0160775



(a) sea-swell energy equivalent (Case E, SSER=1.0)



(b) swell-dominated (Case AK, SSER=0.09)



(c) wind-sea-dominated (Case AO, SSER=3.66)

Fig. 15 Relations between wave group steepness and kurtosis in crossing sea states considering various crossing angles.

4.4 Exceedance probability of wave height at maximum kurtosis

Generally, kurtosis is closely related to large waves. The larger the kurtosis, the steeper the wave height distribution, and the greater probability of extreme waves. Fig. 16 and Fig. 17 give the exceedance probability of wave height at maximum kurtosis in multi-directional sea states, with Rayleigh distribution for reference. The

MER distribution is obtained from the unidirectional sea state under the assumption of the equivalent energy. In unimodal sea states (Fig. 16), it turned out as expected that Rayleigh distribution underestimates the statistical wave height. Further, as the directional distribution becomes narrower, the deviation from the Rayleigh distribution gradually increases, especially in the range of $1.5 < H/H_s < 2.0$. But statistical data are still below the prediction obtained from MER distribution. That is, in unimodal sea states the wave height distribution lies between the Rayleigh distribution and MER distribution, and the narrower the directional distribution width, the closer the statistical wave height distribution is to the MER distribution.

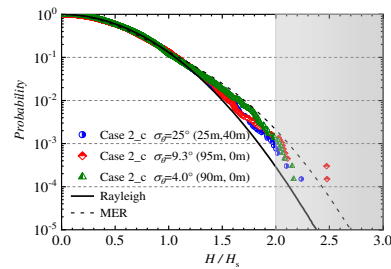
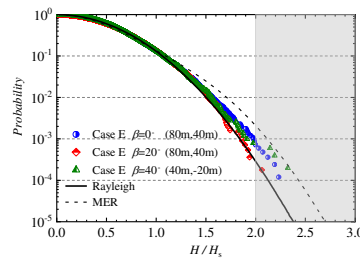
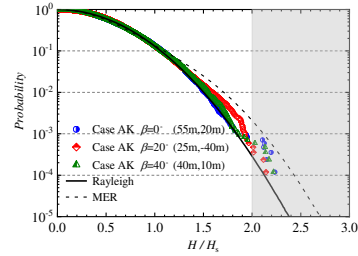


Fig. 16 Exceedance probability of wave height at maximum kurtosis in unimodal sea states considering various directional distribution widths.

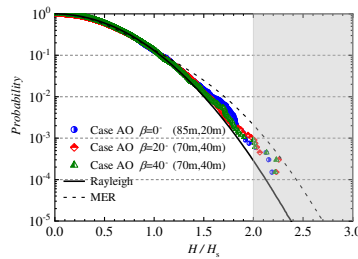
Similarly, the statistical wave height distributions in the crossing sea states are also between the Rayleigh distribution and the corresponding MER distribution, shown in Fig. 17. Under the sea-swell energy equivalent configuration (Fig. 17a), as the crossing angle β increases from 0° to 40° , the wave height probability distributed in the range of $1.5 < H/H_s < 2.0$ changes a little and is quite close to the Rayleigh distribution, whereas, in the range of $H/H_s > 2.0$, the tail of the exceedance probability deviates from the Rayleigh distribution, revealing the underestimation of the wave height distribution of large wave events. Especially when $\beta=40^\circ$, the value of H/H_s can reach up to 2.3, at which point the statistical wave height distribution is close to the value predicted by MER distribution. Under the swell-dominated (Fig. 17b) and wind-sea-dominated configuration (Fig. 17c), the wave height distribution changes a little with the increase of the crossing angle from 0° to 40° . It delivers the information that the crossing angle has little effect on the statistical wave height distributions at the maximum kurtosis position of the sea state dominated by swell or wind-sea.



(a) sea-swell energy equivalent (Case E, SSER=1.0)



(b) swell-dominated (Case AK, SSER=0.09)



(c) wind-sea-dominated (Case AO, SSER=3.66)

Fig. 17 Exceedance probability of wave height at maximum kurtosis in crossing sea states considering various crossing angles.

4.5 Exceedance probability of wave crest at maximum kurtosis

Under the assumption of linear theory, wave crest distribution is consistent with the wave height distribution. However, in the real sea state, the nonlinear multi-directional waves lead to the asymmetric of the wave crest and wave trough. Wave crest distribution should be further studied. Fig. 18 and Fig. 19 show the exceedance probability of wave crest at maximum kurtosis in multi-directional sea states.

In unimodal sea states (Fig. 18), the Rayleigh distribution underestimates the statistical wave crest. The narrower the directional distribution width, the greater the deviation from the Rayleigh distribution. But these statistical wave crest distributions are close to the Forristall distribution with the second-order theory involved. It can be roughly concluded that in a unimodal sea state, directional distribution weakened the higher-order (third- and more than third-order) effect on the wave crest so that the Forristall distribution can approximate the wave crest distribution.

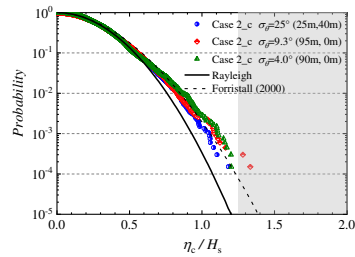
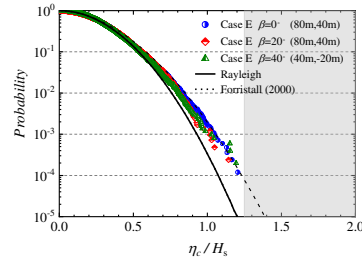
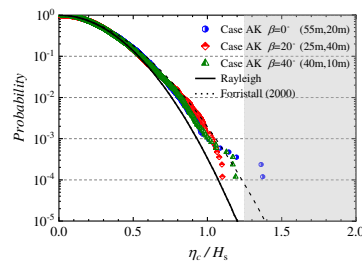


Fig. 18 Exceedance probability of wave crest at maximum kurtosis in unimodal sea states considering various directional distribution widths.

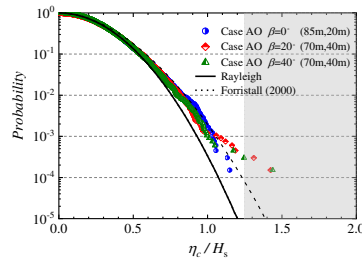
In crossing sea states (Fig. 19), except for a very small amount of scatters exceeding the predictive distribution in the tail, the statistical wave crest distribution can be predicted by the Forristall distribution, which is similar to the observation in the unimodal sea state. Contrary to the phenomenon of wave height distribution, there are some larger wave crests under the swell-dominated (Fig. 19b) and wind-sea-dominated (Fig. 19c) configuration. It reflects that crossing sea state is a more complex undergoing with strong nonlinearity. Delimiting the extreme wave occurrence only by the wave height distribution is inaccurate, manifesting the urgent need that the wave crest distribution is essential when it comes to the crossing sea state.



(a) sea-swell energy equivalent (Case E, SSER=1.0)



(b) swell-dominated (Case AK, SSER=0.09)



(c) wind-sea-dominated (Case AO, SSER=3.66)

Fig. 19 Exceedance probability of wave crest at maximum kurtosis in crossing sea states considering various crossing angles.

5. Conclusions

Unimodal-spectrum-multi-direction sea states and bimodal-spectrum-multi-direction sea states are simulated in a numerical wave basin based on High Order Spectral (HOS) method. The influences of the directional

1 distribution and energy distribution on nonlinear statistics are studied in crossing sea states, along with those in
2 unimodal sea states for reference. The main conclusions are as follows:

- 3 (1) The spatial evolutions of kurtosis in a three-dimensional field are first given. In sea-swell energy
4 equivalent sea state, the larger the crossing angle, the more inhomogeneous the spatial evolution of
5 kurtosis, the larger the maximum values of kurtosis, and the more the maximum value occurs. When the
6 energy distribution is asymmetric, i.e., swell-dominated or wind-sea-dominated state, the crossing angle
7 has little effect on the spatial evolutions of kurtosis.
- 8 (2) A positive linear correlation is observed between wave group steepness and kurtosis in unimodal sea state,
9 while not available in crossing sea state characterized by bimodal spectrum.
- 10 (3) The threshold of the exceedance probability of wave height distributions in multi-direction sea states is
11 the MER prediction, which is obtained from the unidirectional configuration assuming equivalent energy.
- 12 (4) The Forristall distribution based on second-order theory can roughly estimate the wave crest distribution
13 in multi-directional sea states irrespective of the spectral type.
- 14 (5) Crossing sea state is a more complex undergoing. To estimate the probability of extreme wave occurrence,
15 both wave height distribution and wave crest distribution are certainly essential.

16 Acknowledgements

17 This work is supported by the National Natural Science Foundation of China (52071096, 52201322), the
18 National Natural Science Foundation of China National Outstanding Youth Science Fund Project (52222109),
19 Guangdong Basic and Applied Basic Research Foundation (2022B1515020036), Guangzhou Basic and Applied
20 Basic Research Foundation (2023A04J1596), the Fundamental Research Funds for the Central Universities
21 (2022ZYGXZR014, 2022ZYGXZR034), the Funds of Guangxi Key Laboratory of Beibu Gulf Marine
22 Resources, Environment and Sustainable Development (NRES-2023-804), and EPSRC (EP/V050079/1).

24 AUTHOR DECLARATION

25 Conflict of Interest

26 The authors have no conflicts to disclose.

27 Author Contributions

28 **Lei Wang:** Conceptualization (lead); Methodology (lead); Data curation (lead); Formal analysis (lead);
29 Investigation (lead); Writing – original draft (lead), Writing – review & editing (equal).; **Kanglixi Ding:**
30 Investigation (equal); Visualization (equal). **Binzhen Zhou:** Funding acquisition (lead); Project administration
31 (lead); Supervision (equal); Writing – review & editing (equal). **Peng Jin:** Visualization (equal); Writing –
32 review & editing (equal). **Shuxue Liu:** Conceptualization (equal); Methodology (equal); Supervision (equal);
33 **Jinghua Wang:** Methodology (equal); Writing – review & editing (equal). **Tianning Tang:** Methodology
34 (equal); Writing – review & editing (equal).

36 DATA AVAILABILITY

37 The data that support the findings of this study are available from the corresponding author upon reasonable
38 request.

39

Appendix: HOS method

Based on the potential flow theory, the fluid is assumed to be incompressible, inviscid, and irrotational. The velocity potential $\Phi(x, z, t)$ inside the two-dimensional domain at a preset position (x, z) satisfies the Laplace equation

$$\nabla^2 \Phi(x, y, z, t) = 0 \quad (20)$$

in which $\nabla = (\partial/\partial x, \partial/\partial y, \partial/\partial z)$.

In the advanced HOS model [47], the velocity potential $\Phi(x, y, z, t)$ can be solved as a sum of the free surface spectral potential $\Phi_f(x, y, t)$ and the additional velocity potential $\Phi_{add}(x, y, z, t)$ [48].

$$\eta_t = (1 + |\nabla_x \eta|^2) (\Phi_f)_z + (\Phi_{add})_z - \nabla_x (\Phi_f + \Phi_{add}) \cdot \nabla_x \eta \quad z = \eta(x, y, t) \quad (21)$$

$$\begin{aligned} (\Phi_f)_t &= -g\eta - \frac{1}{2} (\nabla_x \Phi_f)^2 + \frac{1}{2} (1 + |\nabla_x \eta|^2) [(\Phi_f)_z]^2 - (\Phi_{add})_t \\ &\quad - (\nabla_x \Phi_f) \cdot (\nabla_x \Phi_{add}) - \frac{1}{2} (\nabla_x \Phi_{add})^2 - \frac{1}{2} [(\Phi_{add})_z]^2 \quad z = \eta(x, y, t) \end{aligned} \quad (22)$$

Accordingly, the free surface spectral potential $\Phi_f(x, y, t)$ satisfies the Laplace equation, the free surface boundary conditions, and the bottom condition, and the additional velocity potential $\Phi_{add}(x, y, z, t)$ satisfies the Laplace equation, the wave-maker boundary condition, and the bottom condition.

The convergence analysis is carried out with the parameters: $N_z = N_d/4$, $M=5$, and the result of the convergence analysis with respect to the number of points per peak wavelength N_{Lp} is represented in Fig. 20. The figure displays two lines representing the convergence rates of 2 and 3 as a reference. Considering the numerical simulation of the unidirectional irregular wave trains, the overall error is about 5% with 30 points per corresponding peak wavelength. This value of $N_{Lp}=30$ is chosen as a converged parameter for the rest of the study. It ensures the accuracy of the numerical simulation as well as a fast solution. A similar convergence analysis has been conducted for the discretization in time (time-step Δt) as well as the order of nonlinearity of the method M. The final numerical configuration is $N_{Lp}=30$, $T_p/\Delta t=100$, and $M=5$.

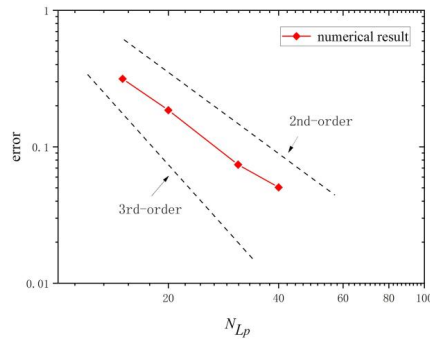


Fig. 20 Convergence of the numerical simulation with respect to the number of points per corresponding peak wavelength.

References

- [1] Onorato M, Osborne A, and Serio M. Modulational instability and non-Gaussian statistics in experimental.

This is the author's peer reviewed, accepted manuscript. However, the online version of record will be different from this version once it has been copyedited and typeset.

PLEASE CITE THIS ARTICLE AS DOI: 10.1063/5.0160775

- 1 *Physics of Fluids*, 2005, 17:1-4.
- 2 [2] Onorato, M, Osborne A, Serio M, Cavaleri L, Brandini C, Stansberg C. Observation of strongly
- 3 non-Gaussian statistics for random sea surface gravity waves. *Physical Review E*, 2004, 70(6): 067302.
- 4 [3] Yu L, Liu S. Random wave and its applications to engineering. 4th Edition, 2011.
- 5 [4] Xie J, Ma Y, Dong G, Perlin M. Numerical investigation of third-order resonant interactions between two
- 6 gravity wave trains in deep water. *Physical Review Fluids*, 2021, 6: 014801.
- 7 [5] Liu S, Waseda T, Yao J, Zhang X. Statistical properties of surface gravity waves and freak wave occurrence
- 8 in crossing sea states. *Physical Review Fluids*, 2022, 7: 074805.
- 9 [6] Waseda T, Kinoshita T, Tamura H. Evolution of a random directional wave and freak wave occurrence.
- 10 *Journal of Physical Oceanography*, 2009, 39(3): 621-639.
- 11 [7] Young I, Van Vledder G. A review of the central role of nonlinear interactions in wind-wave evolution.
- 12 *Proceeding of the Royal Society A Mathematical Physical and Engineering Sciences*, 1993, 342(1666):
- 13 505-524.
- 14 [8] Liu S, Zhang X. Extreme wave crest distribution by direct numerical simulations of long-crested nonlinear
- 15 wave fields. *Applied Ocean Research*, 2019, 86: 141-153.
- 16 [9] Tao A, Zheng J, Chen B, Li H, Peng J. Properties of freak waves induced by two kinds of nonlinear
- 17 mechanisms. *Proceedings of the Coastal Engineering Conference*, 2012, 1.
- 18 [10] Fu R, Wang G, Zheng J, Ma Y. Statistical properties of group energy and group duration for unidirectional
- 19 ocean wave groups. *Ocean Engineering*, 2022, 266: 112786.
- 20 [11] Ochi M, Ocean waves: the stochastic approach. Cambridge University Press, Cambridge, 1998.
- 21 [12] Longuet-Higgins M. On the statistical distribution of the heights of sea waves. *Journal of Marine Research*,
- 22 1952, 11(3): 245-66.
- 23 [13] Henderson D M, Segur H. The role of dissipation in the evolution of ocean swell. *Journal of Geophysical*
- 24 *Research: Oceans*, 2013, 118(10): 5074-5091.
- 25 [14] Rajan G K, Henderson D M. The linear stability of a wavetrain propagating on water of variable depth.
- 26 *SIAM Journal on Applied Mathematics*, 2016, 76(5): 2030-2041.
- 27 [15] Sutherland G, Halsne T, Rabault J, et al. The attenuation of monochromatic surface waves due to the
- 28 presence of an inextensible cover. *Wave Motion*, 2017, 68: 88-96.
- 29 [16] Kharif C, Pelinovsky E. Physical mechanisms of the rogue wave phenomenon. *European Journal of*
- 30 *Mechanics - B/Fluids*, 2003, 22(6):603-634.
- 31 [17] Janssen P A E M. Nonlinear four-wave interactions and freak waves. *Journal of Physical Oceanography*,
- 32 2003, 33: 863-84.
- 33 [18] Mori N, Onorato M, Janssen P A E M, Osborne A, Serio M. On the extreme statistics of long-crested deep
- 34 water waves: theory and experiments. *Journal of Geophysical Research*, 2007, 112.
- 35 [19] Mori N, Janssen P A E M. On kurtosis and occurrence probability of freak waves. *Journal of Physical*
- 36 *Oceanography*, 2006, 36: 1471-83.
- 37 [20] Li Y, Li X. Weakly nonlinear broadband and multi-directional surface waves on an arbitrary depth: A
- 38 framework, Stokes drift, and particle trajectories. *Physics of Fluids*, 2021, 33: 076609.
- 39 [21] Fedele, F. On the kurtosis of deep-water gravity waves. *Journal of Fluid Mechanics*, 2015, 782, 25-36.
- 40 [22] Janssen P A E M, Janssen A J E M. Asymptotics for the long-time evolution of kurtosis of narrow-band
- 41 ocean waves. *Journal of Fluid Mechanics*, 2019, 859: 790-818.
- 42 [23] Tang T, Xu W, Barratt D, Bingham H, Li Y, Taylor P, van den Bremer T, Adcock T. Spatial evolution of the
- 43 kurtosis of steep unidirectional random waves. *Journal of Fluid Mechanics*, 2021, 908, A3.
- 44 [24] Onorato M, Osborne A, Serio M, et al. Freak waves in random oceanic sea states. *Physical Review Letters*,

This is the author's peer reviewed, accepted manuscript. However, the online version of record will be different from this version once it has been copyedited and typeset.

PLEASE CITE THIS ARTICLE AS DOI: 10.1063/5.0160775

- 2001, 86(25): 5831-5834.
- [25] Onorato M, Cavaleri L, Fouques S, et al. Statistical properties of mechanically generated surface gravity waves: a laboratory experiment in a three-dimensional wave basin. *Journal of Fluid Mechanics*, 2009, 627: 235-257.
- [26] Guedes Soares C. Representation of double-peaked sea wave spectra. *Ocean Engineering*, 1984, 11(2):185-207.
- [27] Guedes Soares C. On the occurrence of double peaked wave spectra. *Ocean Engineering*, 1991, 18(1-2):167-171.
- [28] McAllister M, Draycott S, Adcock T, Taylor P, van den Bremer T. Laboratory recreation of the Draupner wave and the role of breaking in crossing seas. *Journal of Fluid Mechanics*, 2018, 860: 767-786.
- [29] Cavaleri L, Bertotti L, Torrisi L, et al. Rogue waves in crossing seas: The Louis Majesty accident. *Journal of Geophysical Research: Oceans*, 2012, 117(C11).
- [30] Onorato M, Osborne A, Serio M, et al. Extreme waves, modulational instability and second order theory: wave flume experiments on irregular waves. *European Journal of Mechanics - B/Fluids*, 2006, 25(5): 586-601.
- [31] Grönlund A, Eliasson B, Marklund M. Evolution of rogue waves in interacting wave systems. *Europhysics Letters*, 2009, 86(2): 24001.
- [32] Regev A, Agnon Y, Stiassnie M, et al. Sea-swell interaction as a mechanism for the generation of freak waves. *Physics of Fluids*, 2008, 20(11): 112102.
- [33] Gramstad O, Trulsen K. Can swell increase the number of freak waves in a wind-sea? *Journal of Fluid Mechanics*, 2010, 650: 57-79.
- [34] Toffoli A, Bitner-Gregersen E, Osborne A, Serio M, Monbaliu J, Onorato M. Extreme waves in random crossing seas: laboratory experiments and numerical simulations. *Geophysical Research Letters*, 2011, 38: L06605.
- [35] Ochi M, Hubble E. Six parameter wave spectra. *15th International Conference on Coastal Engineering*, Honolulu, Hawaii, United States, 1976.
- [36] Longuet-Higgins M, Cartwright D, Smith N. Observations of the directional spectrum of sea waves using the motions of a floating buoy. Englewood Cliffs, N. J. USA: In *Ocean Wave Spectra*, Prentice-hall Inc, 1963.
- [37] Zhang H, Liu S, Li J, et al. Interactions between multi-directional irregular waves and a pile group in a side-by-side arrangement: Statistical analysis. *Coastal Engineering*, 2019, 147: 115-134.
- [38] Rodriguez G, Guedes Soares C, Pacheco M, et al. Wave height distribution in mixed sea states. *Journal of Offshore Mechanics and Arctic Engineering*, 2002, 124:34-40.
- [39] Li J, Liu S. Focused wave properties based on a high order spectral method with a non-periodic boundary. *China Ocean Engineering*, 2015, 29(1):1-16.
- [40] Wang L, Li J, Liu S, Ducroz G. Statistics of long-crested extreme waves in single and mixed sea states. *Ocean Dynamics*. 2020; 71(1): 21-42.
- [41] Wang L, Ding K, Zhou B, Li J, Liu S, Tang T. Quantitative prediction of the freak wave occurrence probability in co-propagating mixed waves. *Ocean Engineering*, 2023, 271: 113810.
- [42] Ducroz G, Bonnefoy F, Le Touzé D, Ferrant P. A modified High-Order Spectral method for wavemaker modeling in a numerical wave tank. *European Journal of Mechanics - B/Fluids*, 2012; 34: 19-34.
- [43] Dong G, Ma Y, Ma X. Cross-shore variations of wave groupiness by wavelet transform. *Ocean Engineering*, 2008, 35(7): 674-684.
- [44] Forristall G. Wave crest distributions: observations and second-order theory. *Journal of Physical*

This is the author's peer reviewed, accepted manuscript. However, the online version of record will be different from this version once it has been copyedited and typeset.

PLEASE CITE THIS ARTICLE AS DOI: 10.1063/5.0160775

- 1 *Oceanography*, 2000, 30(8): 1931-1943.
- 2 [45] Wang L, Zhou B, Jin P, Li J, Liu S, Ducroz G. Relation between occurrence probability of freak waves
- 3 and kurtosis/skewness in unidirectional wave trains under single-peak spectra. *Ocean Engineering*, 2022;
- 4 248(15): 110813.
- 5 [46] Toffoli A, Bitner-Gregersen E M, Osborne A R, et al. Extreme waves in random crossing seas: Laboratory
- 6 experiments and numerical simulations. *Geophysical Research Letters*, 2011, 38(6).
- 7 [47] Agnon Y, Bingham H B. A non-periodic spectral method with application to nonlinear water waves.
- 8 *European Journal of Mechanics-B/Fluids*, 1999, 18(3): 527-534.
- 9 [48] Ducroz G, Bonnefoy F, Le Touzé D, et al. A modified high-order spectral method for wavemaker
- 10 modeling in a numerical wave tank. *European Journal of Mechanics-B/Fluids*, 2012, 34: 19-34.